Contents lists available at ScienceDirect

Annals of Nuclear Energy

journal homepage: www.elsevier.com

Measurement uncertainty of rossi-alpha neutron experiments

Michael Y. Hua [a, b], Jesson D. Hutchinson [b], George E. McKenzie [b], Brian C. Kiedrowski [a], Michael W. Liemohn [c], Shaun D. Clarke [a], Sara A. Pozzi [a]

[a] Department of Nuclear Engineering and Radiological Sciences, University of Michigan, Ann Arbor, MI 48109, United States
[b] NEN-2: Advanced Nuclear Technology Group, Los Alamos National Laboratory, Los Alamos, NM 87545, United States
[c] Department of Climate and Space Sciences and Engineering, University of Michigan, Ann Arbor, MI 48109, United States

ARTICLE INFO

Article history:
Received 20 March 2020
Received in revised form 14 June 2020
Accepted 16 June 2020
Available online xxx

Keywords:
Rossi-alpha
Neutron noise
Prompt neutron decay constant
Prompt period
Subcritical measurements
Uncertainty
Error bars

ABSTRACT

Rossi-alpha neutron experiments are used to estimate the prompt neutron decay constant of a fissile assembly, a quantity of widespread interest in applications including in nuclear nonproliferation and criticality safety. This work develops a mathematical model to efficiently estimate measurement uncertainty of Rossi-alpha neutron experiments inferred from a two-exponential fit model with histogram binning. The derived uncertainty estimates were validated using repeated Rossi-alpha measurements of a subcritical, 4.5-kg sphere of weapons-grade, α-phase plutonium with nickel, copper, tungsten, and polyethylene reflectors. The estimates of uncertainty for the histogram data produced by the model were conservative and agree with the reference uncertainties within noise. The estimates of the prompt neutron decay constant uncertainty agreed with the reference uncertainties within one standard deviation. The proposed model will reduce total measurement times, ultimately reducing operational and procedural costs in application.

1. Introduction

Subcritical analyses are used for many applications including nuclear nonproliferation and criticality safety (Uhrig and Commission, 1970; Doyle, 2019). The prompt neutron decay constant or its negative reciprocal, the prompt period, are typically quantities of interest when measuring near- or delayed-critical assemblies of fissile material. The Rossi-alpha method, based on observing the nonrandom neutron time correlations in neutron-multiplying media, is one modality to measure the prompt neutron decay constant that involves fitting histogram data with a nonlinear least squares algorithm (Feynman et al., YYYY; Feynman et al., YYYY; Feynman et al., 1956; Orndoff, 1957). The correlated portion of Rossi-alpha histogram is traditionally fit with a single decaying exponential, though recent work has demonstrated that a two-exponential model is more adequate (Kuramoto et al., 2006; Hutchinson et al., 2017). The transition to two exponentials arises when the fissile material is reflected. Based on prior works describing reflected assemblies (Avery, 1958; Cohn, 1962), recent work developed the two-exponential model for fitting Rossi-alpha histograms (Hua et al., 2020). Although the method is well understood, Rossi-alpha experiments are deficient in rigorous and efficient quantification of measurement uncertainty.

In this work, uncertainty propagation is analytically derived for Rossi-alpha measurements and a quasi-analytic method for determining vertical error bars for the histogram is developed. Currently, there are two main methods to estimate uncertainty.

method one. Repeat a single Rossi-alpha experiment many times to obtain many values of the prompt neutron decay constant. Estimate the uncertainty by taking the sample standard deviation of the values.
method two. Use the standard deviation provided by the unweighted nonlinear least squares fit algorithm.

Method one requires long total measurement times to precisely estimate the uncertainty. This work develops uncertainty propagation from histogram error bars to the uncertainty in the prompt neutron decay constant and a new analytic method to infer histogram error bars that does not rely on repeated measurements. Inferring uncertainty from one measurement reduces the total measurement time and therein results in reduced procedural and operational costs.

Unlike method one, method two is different for the one- and two-exponential models. In the one-exponential model, the prompt neutron decay constant is a fit parameter, whereas the quantity is a combination of fit parameters in the two-exponential model. Thus, while taking the fit uncertainty is straightforward for the one-exponential model, the uncertainty must be propagated when the two-exponential model is used. Furthermore, simply taking the fit uncertainty does not consider the uncertainty in the data unless the fit is weighted. The uncertainty propagation developed in this work propagates uncertainty by way of weights and propagates uncertainty from the two-exponential fit parameters to the prompt neutron decay constant.

The theory developed in this work is validated with organic scintillator and ^{3}He gas proportional counter measurements of a 4.5 kg sphere of alpha-phase, weapons-grade plutonium reflected by tungsten, copper, nickel, and polyethylene; the new method is com-

https://doi.org/10.1016/j.anucene.2020.107672
0306-4549/

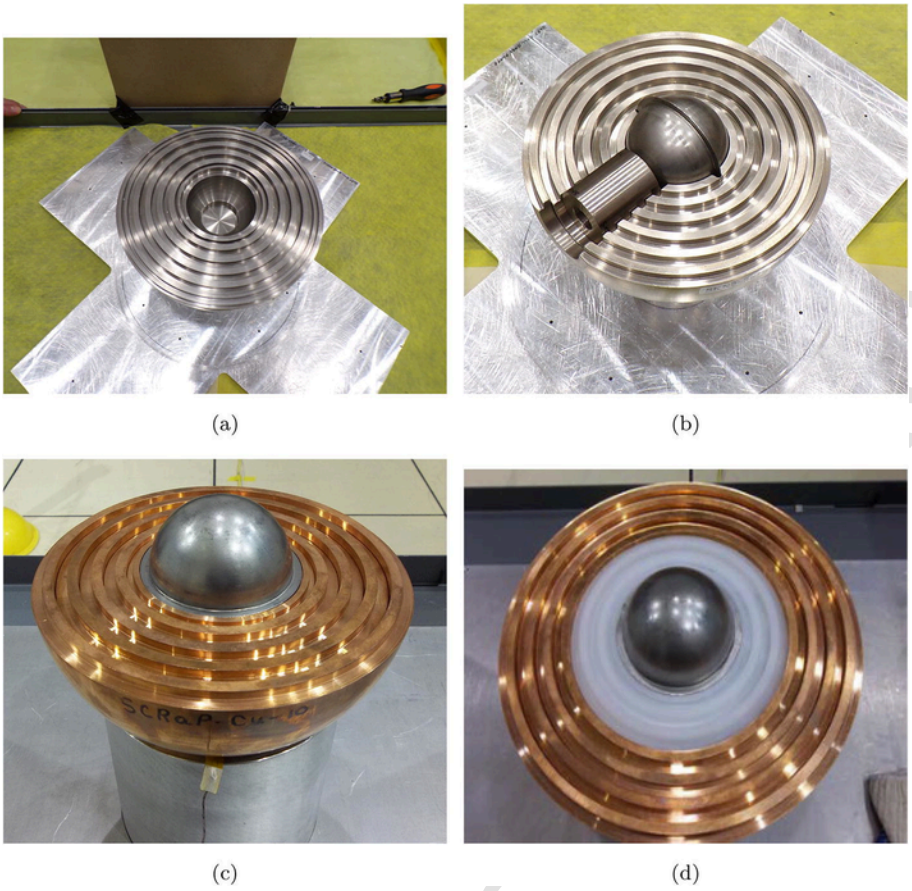

Fig. 1. Configurations used in the experiments. The BeRP ball is reflected by 7.62 cm of tungsten, nickel, or copper shown in Fig. 1a–c, respectively. Fig. 1d shows the BeRP ball reflected by 3.81 cm of polyethylene and 5.08 cm of copper.

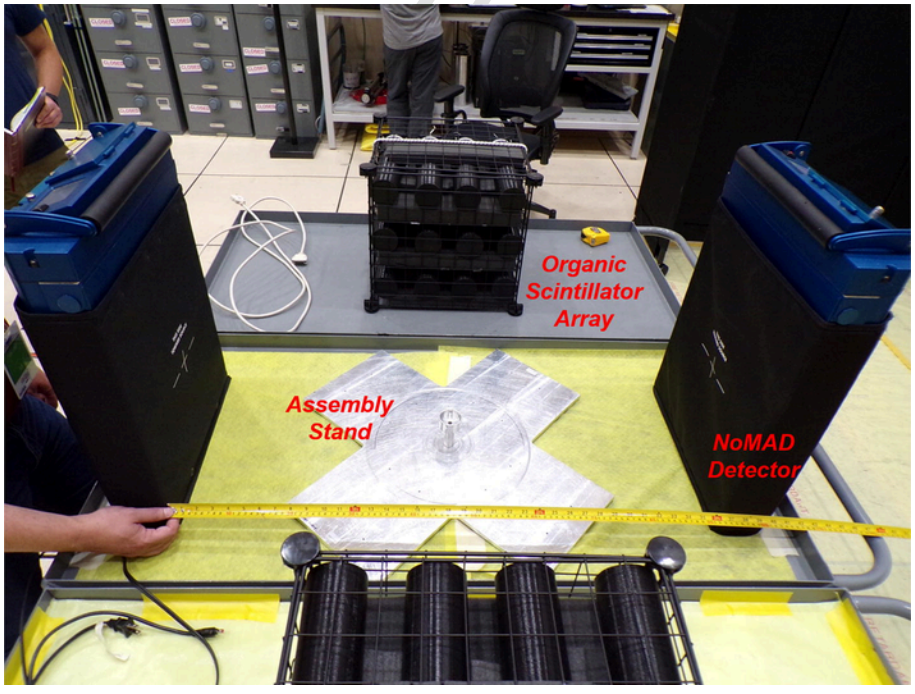

Fig. 2. Photo of the experimental setup for the organic scintillator measurements.

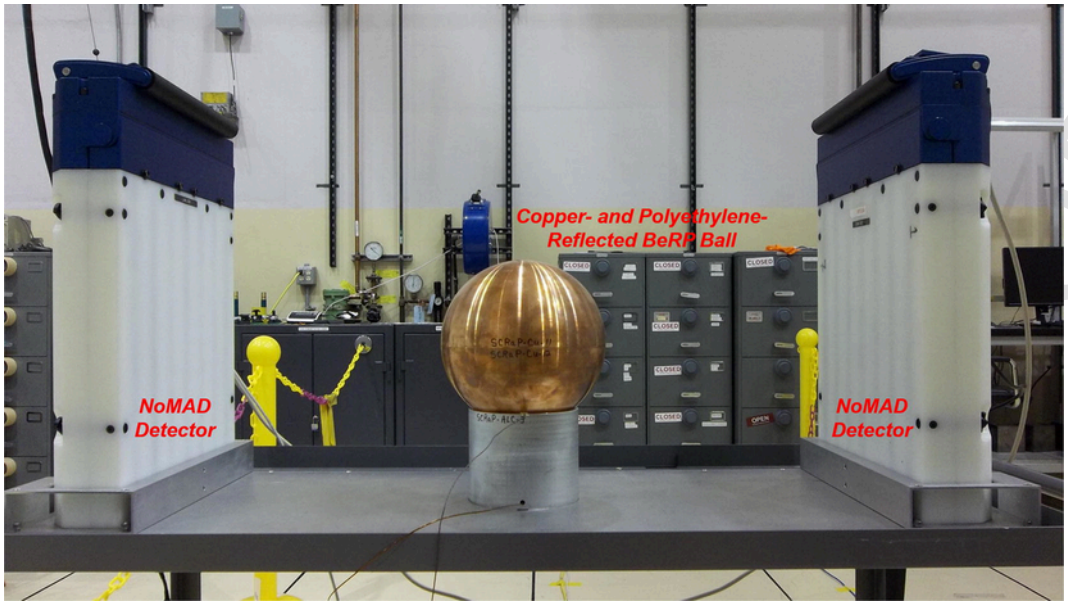

Fig. 3. Photo of the experimental setup for the ^{3}He measurements.

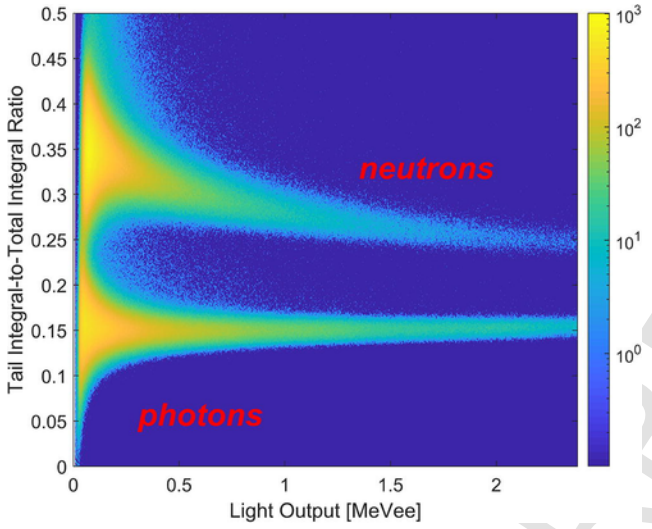

Fig. 4. Pulse shape discrimination plot for the organic scintillator measurement of the copper-reflected plutonium.

pared to the sample standard deviation method and accuracy-improvement due to weighting is demonstrated.

The structure of this paper is as follows. Background on the Rossi-alpha method is given in Section 2, while the theory of the uncertainty analysis is developed in Section 3. Measured data from the experimental setups described in Section 4 and data analysis explained in Section 5 are used to validate the theory in Section 6, and Section 7 concludes this paper.

2. The Rossi-alpha Method

The purpose of Rossi-alpha measurements is to estimate α, the prompt neutron decay constant, or its negative reciprocal, the prompt period. Prompt neutrons born from fission are correlated in time: the emission is effectively instantaneous and the neutrons can sustain fission chains by inducing further fissions. During the experiment, neutrons are detected and the times of detection are recorded. While Rossi-alpha experiments are traditionally conducted with ^{3}He-gas proportional counters that detect thermal neutrons through capture, recent work has validated and shown increased capabilities with organic scintillators that detect neutrons through scatter (Hua et al., 2020). In post processing, the time differences between any and all neutron detections less than a given reset time are calculated. Note that the reset time is typically larger than typical fission chain durations and much shorter than the half life of the first delayed precursor group. A histogram of the time differences is constructed and fit with

$$p(t)\ dt = A\ dt + Be^{\alpha t}\ dt, \tag{1}$$

the traditional, one-exponential model (Feynman et al., YYYY; Feynman et al., YYYY; Feynman et al., 1956; Orndoff, 1957). The A term represents the uniform probability of uncorrelated counts, and the B term represents the correlated counts that exponentially decay as fission chains die out. Note that Section 5 provides further details on the binning and fitting analyses used in this paper. Prior work (Kuramoto et al., 2006; Hutchinson et al., 2017) experimentally confirmed that a two-exponential fit is more-adequate for assemblies containing reflectors or moderators, and recent work (Hua et al., 2020) derived the two-region-point-kinetics model, in which histograms are fit with

$$\begin{aligned} p(t)\ dt &= A\ dt + B\left[\rho_1 e^{r_1 t} + \rho_2 e^{r_2 t}\right]\ dt. \\ &= A\ dt + \left[\left(B\rho_1\right)e^{r_1 t} + \left(B\rho_2\right)e^{r_2 t}\right]\ dt. \end{aligned} \tag{2}$$

The A and B terms still represent the uncorrelated and correlated counts, respectively, and B scales the coefficients of the two exponentials given by

$$\rho_1 = \frac{(1-R)^2}{r_1} + \frac{2(1-R)(R)}{r_1 + r_2} \tag{3a}$$

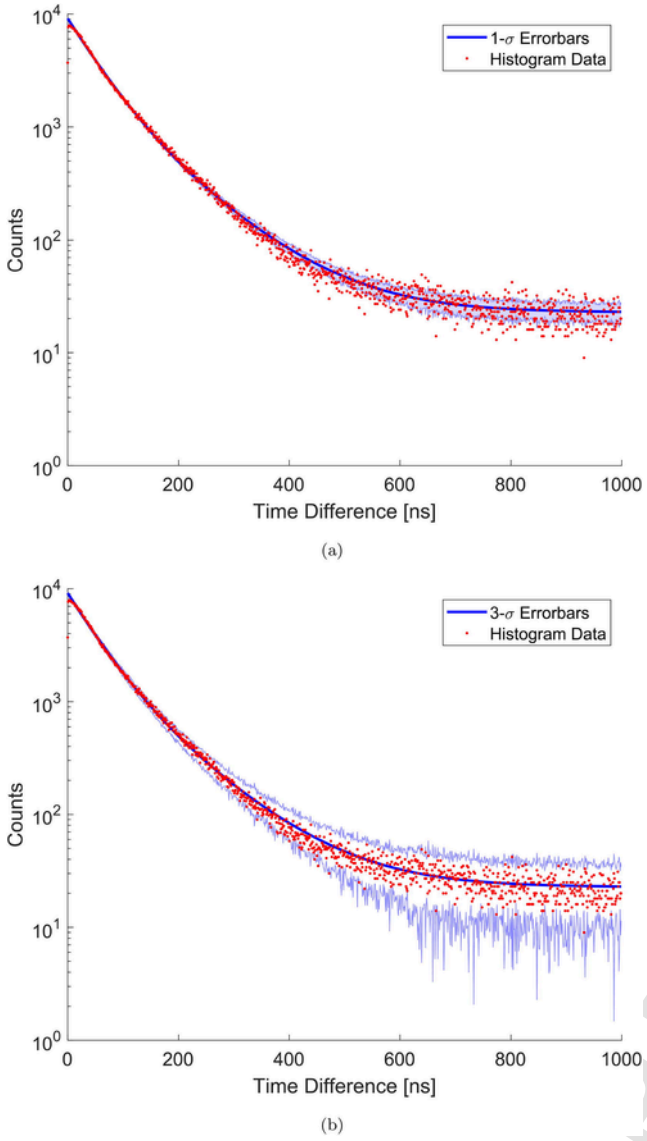

Fig. 5. Rossi-alpha histograms for the organic scintillator measurement of the copper-reflected plutonium with error bars calculated from the sample variance method. The solid, blue line through the center of the red data points is the mean histogram value of the 20 measurements, and the blue region about the center line represent one or three standard deviation error bars. Fig. 5a shows one standard deviation error bars, whereas Fig. 5b shows three.

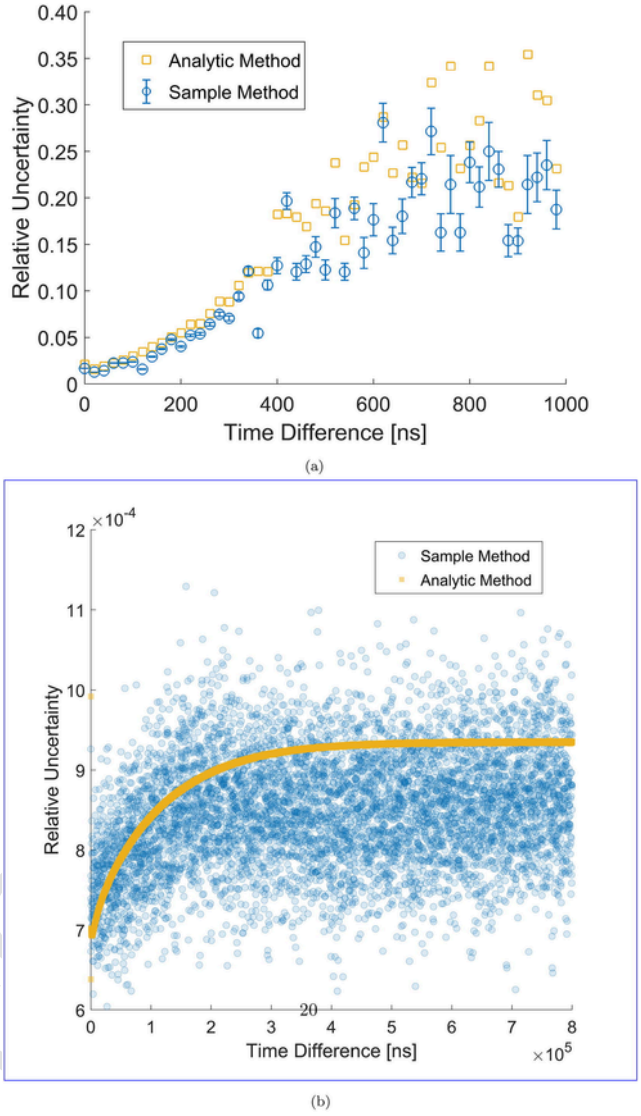

Fig. 6. Direct comparisons of bin-by-bin relative uncertainty estimates between the sample variance and analytic methods for the (a) organic scintillator system measuring the copper-reflected BeRP Ball and (b) ^{3}He system measuring the copper-and-polyethylene-reflected BeRP Ball.

and

$$\rho_2 = \frac{R^2}{r_2} + \frac{2\,(1-R)\,(R)}{r_1 + r_2}. \tag{3b}$$

The coefficients ρ_1 and ρ_2 are functions of the two exponents, r_1 and r_2, and R. Note that r_1 and r_2 are negative, therein representing exponential decay. In the two-exponential model, α is a linear combination of the two exponents and R is the linear parameter between zero and one. The equation for R and the linear equation for α is given by

$$R = \frac{r_1 - \alpha}{r_1 - r_2} \tag{4a}$$

or rewritten as

$$\alpha = r_1\,(1-R) + r_2\,(R)\,. \tag{4b}$$

Derivations for Eqs. (3) and (4) are shown in Ref. Hua et al. (2020).

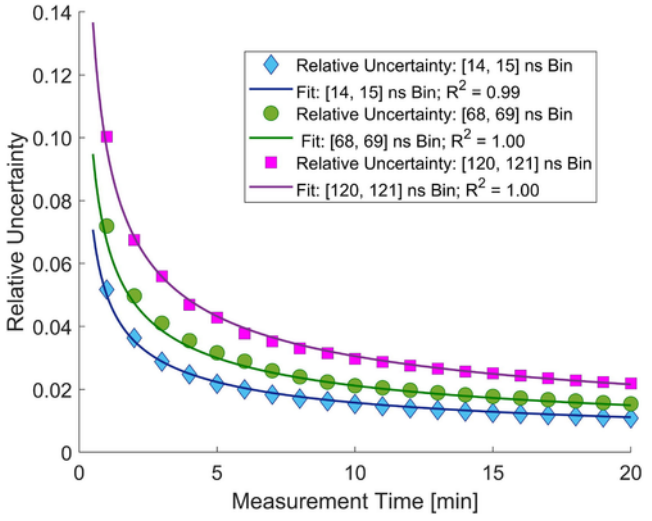

Fig. 7. Relative uncertainty as a function of measurement time in three bins, $y = Ax^{-.5}$ fits for each data series, and R^2 values for the fits for the organic scintillator measurement of the copper-reflected BeRP Ball.

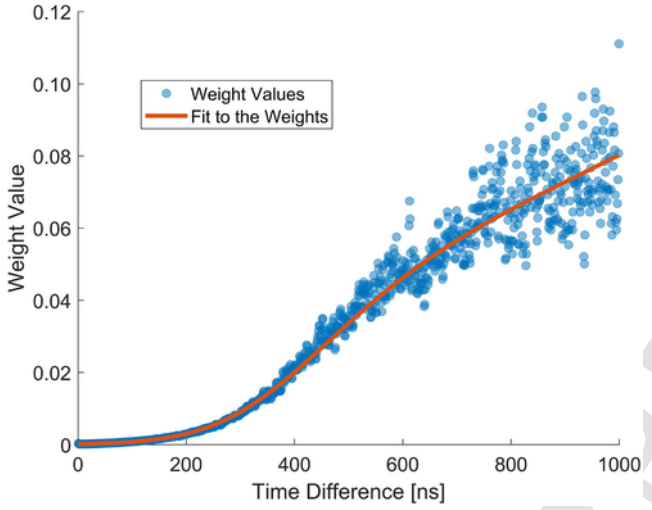

Fig. 8. Sample weights with a fit for the organic scintillator measurement of the copper-reflected BeRP Ball.

3. Theory

3.1. Uncertainty propagation from fit parameters to point kinetics parameters

The uncertainty in fit parameters is an output of many fitting algorithms; in this work, a nonlinear least squares algorithm is used. When Rossi-alpha histograms are fit with the one-exponential model (Eq. (1)), α is a fit parameter and therefore σ_α is an output. When Rossi-alpha histograms are fit with the two-exponential model (Eq. (2)), $\alpha = \alpha\left(r_1, r_2, B\rho_1, B\rho_2\right)$ is calculated from the fit parameters and therefore the uncertainties in the fit parameters must be propagated to obtain σ_α. In this subsection, given variances in and covariances between the fit parameters, equations are derived to propagate uncertainty to α. For notational simplicity,

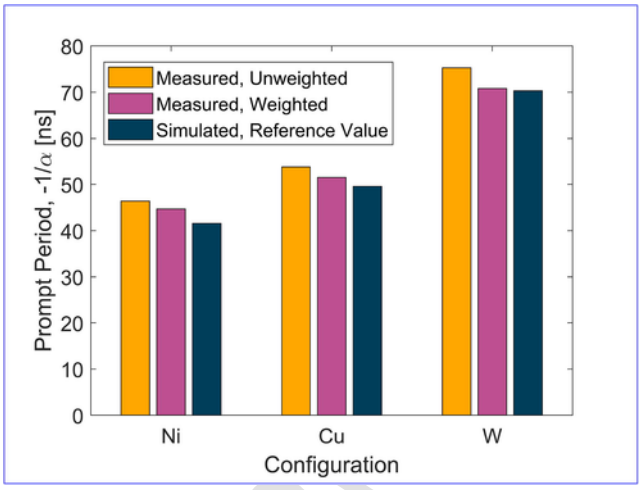

Fig. 9. Estimates of the prompt period with unweighted and weighted fits, and the simulated reference value.

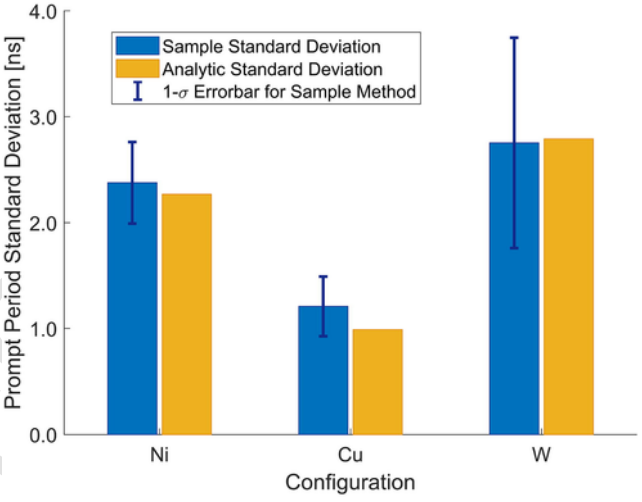

Fig. 10. Standard deviations of the prompt-period estimates obtained from the sample variance and analytic methods.

$$P_1 = B\rho_1 \tag{5a}$$

and

$$P_2 = B\rho_2. \tag{5b}$$

The value of α is expressed in terms of the fit parameters; namely, R is eliminated in Eq. (4b) by independently solving for R and substituting. The measured values P_1 and P_2 in Eq. (5) depend on B,r_1, and r_2 by substituting in Eq. (3) for ρ_1 and ρ_2. The values of r_1 and r_2 are known from the fit, thus an expression for R in terms of known values is obtained by taking the ratio of Eqs. (5a) and (5b). Only one of Eqs. (5a) and (5b) would be needed to determine R if the fitting algorithm returned values for ρ_1 and ρ_2; however, both are needed

to eliminate the scaling term, B. The resulting equation is

$$R = \frac{-r_2\left(r_1P_1 + r_2P_2\right) \pm \sqrt{r_1r_2\left(r_2P_1 + r_1P_2\right)\left(r_1P_1 + r_2P_2\right)}}{\left(r_1 - r_2\right)\left(r_1P_1 + r_2P_2\right)}. \quad (6)$$

Taking the $+$ in $\pm$ results in the physical value of R between 0 and 1. Subsequently substituting Eq. (6) into Eq. (4b) results in

$$\alpha = \left(r_1 + r_2\right) + \sqrt{r_1r_2\frac{\left(P_2r_1 + P_1r_2\right)}{\left(P_1r_1 + P_2r_2\right)}}. \quad (7)$$

Accounting for first-order covariance, the variance in α is:

$$\begin{aligned}\sigma_\alpha^2 \quad = &\left(\frac{\partial\alpha}{\partial r_1}\right)^2\sigma_{r_1}^2 + \left(\frac{\partial\alpha}{\partial r_2}\right)^2\sigma_{r_2}^2 + \left(\frac{\partial\alpha}{\partial P_1}\right)^2\sigma_{P_1}^2 + \left(\frac{\partial\alpha}{\partial P_2}\right)^2\sigma_{P_2}^2 \\ &+2\left(\frac{\partial\alpha}{\partial r_1}\right)\left(\frac{\partial\alpha}{\partial r_2}\right)\sigma_{r_1r_2} \\ &+2\left(\frac{\partial\alpha}{\partial r_1}\right)\left(\frac{\partial\alpha}{\partial P_1}\right)\sigma_{r_1P_1} + 2\left(\frac{\partial\alpha}{\partial r_1}\right)\left(\frac{\partial\alpha}{\partial P_2}\right)\sigma_{r_1P_2} \\ &+2\left(\frac{\partial\alpha}{\partial r_2}\right)\left(\frac{\partial\alpha}{\partial P_1}\right)\sigma_{r_2P_1} + 2\left(\frac{\partial\alpha}{\partial r_2}\right)\left(\frac{\partial\alpha}{\partial P_2}\right)\sigma_{r_2P_2} \\ &+2\left(\frac{\partial\alpha}{\partial P_1}\right)\left(\frac{\partial\alpha}{\partial P_2}\right)\sigma_{P_1P_2}\end{aligned} \quad (8)$$

The partial derivatives in Eq. (8) are:

$$\frac{\partial\alpha}{\partial r_1} = 1 + \frac{P_2r_2\left(2P_2r_1r_2 + P_1\left(r_1^2 + r_2^2\right)\right)}{\delta} \quad (9a)$$

$$\frac{\partial\alpha}{\partial r_2} = 1 + \frac{P_1r_1\left(2P_1r_1r_2 + P_2\left(r_1^2 + r_2^2\right)\right)}{\delta} \quad (9b)$$

$$\frac{\partial\alpha}{\partial P_1} = \frac{P_2r_1r_2\left(r_2^2 - r_1^2\right)}{\delta} \quad (9c)$$

$$\frac{\partial\alpha}{\partial P_2} = \frac{P_1r_1r_2\left(r_1^2 - r_2^2\right)}{\delta} \quad (9d)$$

where

$$\delta = 2\sqrt{r_1r_2\left(P_2r_1 + P_1r_2\right)\left(P_1r_1 + P_2r_2\right)^3}. \quad (9e)$$

Thus, given the uncertainties in the fit parameters, typically in the form of the variance–covariance matrix, the uncertainty in α is obtained from Eq. (8). Section 3.2 outlines how to obtain the variance–covariance matrix.

3.2. Uncertainty in fit parameters

Suppose a fit with P number of parameters is applied to a histogram with N number of bins/data points using least squares regression. The Jacobian, J, of the fit is an $[N\times P]$ matrix and is an available output of the fitting algorithm. If the fit is not weighted, the variance–covariance matrix, Σ, of the fit parameters is given by

$$\Sigma = (\mathrm{RMSE})^2\left[J^TJ\right]^{-1}, \quad (10)$$

where RMSE is the root mean square error (Albritton et al., 1976). The diagonal of the variance–covariance matrix contains the variances of the fit parameters, and the off-diagonal terms contain the covariances. If the fit is weighted by the $[N\times N]$ matrix

$$\begin{aligned}W &= \begin{bmatrix} w_{1,1} & 0 & \cdots & 0 \\ 0 & w_{2,2} & \cdots & 0 \\ \vdots & \vdots & \ddots & \vdots \\ 0 & 0 & \cdots & w_{N,N}\end{bmatrix} \\ &= \begin{bmatrix} \frac{1}{\sigma_{1,1}^2} & 0 & \cdots & 0 \\ 0 & \frac{1}{\sigma_{2,2}^2} & \cdots & 0 \\ \vdots & \vdots & \ddots & \vdots \\ 0 & 0 & \cdots & \frac{1}{\sigma_{N,N}^2},\end{bmatrix}\end{aligned} \quad (11)$$

where $\sigma_{n,n}^2$ is the variance of the nth bin (therefore $\sigma_{n,n}$ is the error bar), then the variance–covariance matrix is given by Albritton et al. (1976)

$$\Sigma = \left[J^TWJ\right]^{-1}. \quad (12)$$

The choice to use inverse variance weights minimizes the variance in the weighted least squares estimate (Albritton et al., 1976). Section 3.3 describes two methods to obtain the $\sigma_{n,n}$ needed to construct W and weight the fit.

3.3. Bin-by-bin error bars for rossi-alpha histograms

Two ways to calculate vertical error bars, or the standard deviation of the number of counts in each bin, are described in this section. The first, shown in Section 3.3.1, is the sample variance method. The sample variance method uniformly divides a long measurement into many sequential, smaller ones (or uses many identical measurements) and takes the variance of the set of smaller measurements. The second method, called the analytic method, uses the fit to calculate an average time difference and standard deviation for each bin and applies Gaussian smearing (horizontal spread) to infer the vertical error bars.

In this work, the total histogram has N bins, uniform bin widths Δ, left bin edges $t_1,t_2,\ldots,t_N$, fit $p(t)$ of the functional form described in Eq. (2), and histogram values $H_1,H_2,\ldots,H_N$.

3.3.1. Expressions for sample variance method

The error bars in the sample variance method are calculated by taking a bin-by-bin standard deviation between M many independent, identically distributed measurements. The standard deviation in the nth bin (with bin edges $t_n, t_n + \Delta$) σ_n is given by

$$\sigma_n = \sqrt{\frac{1}{M-1}\sum_{m=1}^{M}\left(H_{n,m} - \overline{H}_n\right)^2}, \tag{13}$$

where

$$\overline{H}_n = \frac{1}{M}\sum_{m=1}^{M} H_{n,m}, \tag{14}$$

and $H_{n,m}$ is the histogram value in the nth bin of the mth repeated measurement. The equations given in this subsection are standard definitions of sample mean and standard deviation.

3.3.2. Expressions for analytic method

Heuristically, the analytic approach infers horizontal error bars (compounded uncertainties in the time of neutron detections) from the fit and uses them to estimate vertical error bars due to bin-to-bin spreading. A Gaussian-distributed spread is assumed with bin-specific means and variances calculated from the bin-specific probability density function (obtained from bin-specific normalizations of the fit). A Gaussian distribution is selected based on the high number of counts in each bin and an approximate application of the central limit theorem.

The probability density function for the jth bin $p(t;t_j,\Delta)$ is given by

$$p\left(t;t_j,\Delta\right) = \eta\left(t_j,\Delta\right)p\left(t\right) \quad \text{for} t \in \left[t_j, t_j+\Delta\right), \tag{15}$$

where $\eta(t_j,\Delta)$ is the normalization constant for the jth bin. The normalization constant is obtained by solving

$$1 = \int_{t_j}^{t_j+\Delta} \eta\left(t_j,\Delta\right)\left[A + B\left(e^{r_1 t}\rho_1 + e^{r_2 t}\rho_2\right)\right]dt, \tag{16}$$

which results in

$$\eta\left(t_j,\Delta\right) = \left[A\Delta + B\left(\frac{\rho_1}{r_1}e^{r_1 t_j}\left(e^{r_1\Delta}-1\right) + \frac{\rho_2}{r_2}e^{r_2 t_j}\left(e^{r_2\Delta}-1\right)\right)\right]^{-1}.$$

Given the probability density function, the mean and variance are calculated analytically. The mean is given by

$$\begin{aligned}\mu\left(t_j,\Delta\right) &= \int_{t_j}^{t_j+\Delta} tp\left(t;t_j,\Delta\right)dt \\ &= \eta\left(t_j,\Delta\right)\left[A\Delta\left(t_j+\tfrac{1}{2}\Delta\right) + B\left(m_1+m_2\right)\right],\end{aligned} \tag{18}$$

where

$$m_k = \frac{\rho_k}{r_k^2}\left(e^{r_k\left(t_j+\Delta\right)}\left(r_k\left(t_j+\Delta\right)-1\right) - e^{r_k t_j}\left(r_k t_j - 1\right)\right). \tag{19}$$

The variance is given by

$$\begin{aligned}\sigma^2\left(t_j,\Delta\right) &= \int_{t_j}^{t_j+\Delta} t^2 p\left(t;t_j,\Delta\right)dt - \mu^2 \\ &= \eta\left(t_j,\Delta\right)\left[A\Delta\left(t_j^2 + t_j\Delta + \tfrac{1}{3}\Delta^2\right) + B\left(s_1+s_2\right)\right] \\ &\quad -\mu^2\left(t_j,\Delta\right)\end{aligned} \tag{20}$$

where

$$\begin{aligned}s_k = \frac{\rho_k}{r_k^3}\Big(&e^{r_k\left(t_j+\Delta\right)}\left(\left(r_k\left(\Delta+t_j\right)\right)^2 - 2r_k\left(\Delta+t_j\right)+2\right) \\ &-e^{r_k t_j}\left(\left(r_k t_j\right)^2 - 2r_k t_j + 2\right)\Big).\end{aligned} \tag{21}$$

Using the mean and variance above, the random distribution for the time t in bin j is assumed to be normally distributed as

$$G\left(t;t_j,\Delta\right) = \frac{1}{\sqrt{2\pi\left(x\sigma\left(t_j,\Delta\right)\right)^2}}\exp\left(\frac{-\left(\mu\left(t_j,\Delta\right)-t\right)^2}{2\left(x\sigma\left(t_j,\Delta\right)\right)^2}\right), \tag{22}$$

where x is the number of standard deviations; $x = 1\text{and}3$ correspond to 68.3% and 99.7% confidence intervals, respectively. Note that larger values of x result in diminishing returns by nature of the exponential decay of the Gaussian away from the mean and that any value of $x \geqslant 3.5$ are essentially equivalent. This work arbitrarily uses seven standard deviations, twice the 3.5 limit, which corresponds to a $\left(100 - 3\times10^{-10}\right)$ % confidence interval.

Heuristically, the probability of a bin j count belonging in bin i,$q_i(j)$, is equal to the area under $G(t;t_j,\Delta)$ between the bounds of bin i, $\left[t_i, t_i+\Delta\right)$ (note that $G(t;t_j,\Delta)$ is normalized). The value of $q_i(j)$ is given by

$$q_i\left(j\right) = \int_{t_i}^{t_i+\Delta}\frac{1}{\sqrt{2\pi\sigma^2\left(t_j,\Delta\right)}}\exp\left(\frac{-\left(\mu\left(t_j,\Delta\right)-t\right)^2}{2\sigma\left(t_j,\Delta\right)^2}\right)dt \tag{23}$$

$$= \frac{1}{2}\left[\operatorname{erf}\left(\frac{\left(t_i+\Delta\right)-\mu\left(t_j,\Delta\right)}{\sqrt{2\sigma^2\left(t_j,\Delta\right)}}\right) - \operatorname{erf}\left(\frac{t_i-\mu\left(t_j,\Delta\right)}{\sqrt{2\sigma^2\left(t_j,\Delta\right)}}\right)\right]. \tag{24}$$

The binomial theorem is applied to calculate the variance in bin i due to bin j and summed over all j to get the total variance β_i^2 (and the error bar is β_i). Taken together,

$$\beta_i^2 = \sum_{j=1}^{N} p\left(\mu\left(t_j,\Delta\right)\right)\times q_i\left(j\right)\left(1-q_i\left(j\right)\right). \tag{25}$$

3.4. Uncertainty in error bars for the purpose of validation

This section develops equations for the variance of the variance, Var[Var[X]], where X is a random variable. Error bars from the sample variance and analytic methods will be compared for validation, thus uncertainty or variance of the variance Var[Var[X]] is needed (the content in this subsection is not required for the implementation of the uncertainty analysis). In terms of the moments μ_i (defined by $\mu_i = \mathrm{E}\left[X^i\right]$),

$$\mathrm{Var}\left[\mathrm{Var}\left[X\right]\right] = \mu_4 - 4\mu_3\mu_1 + 8\mu_2\mu_1^2 - \mu_2^2 - 4\mu_1^4. \tag{26}$$

Note that Eq. (26) is a biased estimate of the variance that is adequate for large samples. To give Eq. (26) meaning in the context of this work, the moments for the sample variance and analytic methods must be calculated. The moments for the jth bin in the sample variance method $\mu_i^s(j)$ are

$$\mu_1^s(j) = \frac{1}{M}\sum_{m=1}^{M} H_{j,m}, \tag{27a}$$

$$\mu_2^s(j) = \frac{1}{M} sum_{m=1}^{M} H_{j,m}^2, \tag{27b}$$

$$\mu_3^s(j) = \frac{1}{M}\sum_{m=1}^{M} H_{j,m}^3, \tag{27c}$$

and

$$\mu_4^s(j) = \frac{1}{M}\sum_{m=1}^{M} H_{j,m}^4. \tag{27d}$$

The first four moments for a binomial distribution with n trials and probability p are Papoulis (1984)

$$\mu_1(j) = np, \tag{28a}$$

$$\mu_2(j) = np\left(1 - p + np\right), \tag{28b}$$

$$\mu_3(j) = np\left(1 - 3p + 3np + 2p^2 - 3np^2 + n^2p^2\right), \tag{28c}$$

and

$$\begin{aligned}\mu_4(j) \quad = np\big(&1 - 7p + 7np + 12p^2 - 18np^2 + 6n^2p^2\\ &-6p^3 + 11np^3 - 6n^2p^3 + n^3p^3\big).\end{aligned} \tag{28d}$$

The analytic method assumes a binomial model with $n = p\left(\mu\left(t_j, \Delta\right)\right)$ and $p = q_i(j)$.

4. Experimental setup

A 4.5-kg sphere of weapons-grade, alpha-phase plutonium clad in stainless steel, known as the Beryllium-Reflected Plutonium Ball or BeRP Ball, was measured in four configurations: reflected by 7.62 cm of tungsten, nickel, or copper, or reflected by 3.81 cm of high-density polyethylene and then 5.08 cm of copper. The BeRP Ball (Miller et al., 2011) was used in several benchmarks with the tungsten (Richard et al., YYYY), nickel (Bess and Hutchinson, YYYY; Richard and Hutchinson, YYYY), copper, and heterogeneous reflectors (Hutchinson et al., 2017), all containing comprehensive details on the apparatus and materials; the k_{eff} multiplication factors of the assemblies were 0.948, 0.916, 0.932, and 0.951, respectively (Hua et al., 2020; Hutchinson et al., 2017). Photos of the assemblies with half of the hemishells removed are shown in Fig. 1; note that the nickel reflector in Fig. 1b is completed with cylindrical slugs (Bess and Hutchinson, YYYY; Richard and Hutchinson, YYYY). Measurements were conducted at the National Criticality Experiments Research Center at the Device Assembly Facility within the Nevada National Security Site.

The metal-only assemblies (the tungsten-, nickel-, and copper-reflected BeRP Ball) were measured with an array of 12 5.08 cm × 5.08 cm diameter *trans*-stilbene detectors in a rectangular array 47 cm away from the center of the assemblies. The copper-reflected case was measured for 20 min, and the tungsten and nickel cases were measured for 30 min. The detectors are held in place with a wireframe array and porous foam; the detection system and setup are identical to the one used in Ref. Hua et al. (2020) and a photo is shown in Fig. 2. Although a second organic scintillator array and two ^{3}He-based detection systems were present during the experiment, data used in this work are from only one array.

The heterogeneously-reflected BeRP Ball with high-density polyethylene and copper was measured for 75 min with two Neutron Multiplicity ^{3}He Array Detectors (NoMADs Hutchinson et al., 2017): fifteen ^{3}He tubes embedded in a polyethylene matrix. The front face of the NoMAD detectors were 50 cm from the center of the assembly and the optional cadmium liners were not used; the detection system and setup are identical to the one used in Ref. Hutchinson et al. (2017). (See Fig. 3)

5. Data analysis

Of the raw pulses from the organic scintillator array, clipped pulses (corresponding to light output greater than the range defined during calibration or 2.39 MeVee in this work) and pileup pulses (multiple pulses in the same detector in a 288 ns window) are removed in initial post-processing. Pulse shape discrimination (PSD) is performed to separate neutron and photon pulses since organic scintillators are sensitive to both types of radiation. A charge integration technique is used to perform PSD for discrete energy bands, for every minute, for every detector (Brooks, 1959; Miller et al., 2007; Polack et al., 2015) and the result is the organic scintillator list of neutron detection times. A sample PSD plot is shown in Fig. 4. The NoMADs directly output their list of neutron detection times.

Time differences less than a given reset time are calculated between any and all neutron detections (type-I binning Hansen, YYYY) and a histogram of resultant values is constructed for each configuration. The organic scintillator array uses 1-ns bin widths, whereas the NoMADs use 100-ns bin widths. Each histogram is constant-subtracted by subtracting the mean of the tail and the first $2b + 1$ points are omitted in the fit, where b is the index of the bin with the

most counts. Nonlinear least squares fitting is used to fit Eq. (2) (without the A term, which is accounted for in the constant subtraction) to the histograms and Eq. (4b) is used to calculate α. The methodologies described in Section 3 are used to weight fits (when applicable) and calculate uncertainties.

6. Validation and discussion

For a normal distribution, 68.3% and 99.7% of data are expected to fall within the 1- and 3-σ confidence intervals, respectively. Such confidence intervals were calculated using the sample variance method (20 estimates corresponding to independent 1-min measurements) for the copper-reflected organic scintillator data, shown in Fig. 5; 67.2% and 99.8% of data were respectively contained within the 1- and 3-σ confidence intervals, verifying the sample variance method for bin-by-bin error bars. The analytic bin-by-bin error bars are validated by comparison to those of the sample variance method. The relative uncertainties from both methods are shown in Fig. 6 for both detection systems, using the copper-reflected data for organic scintillators (every 20 data points) and copper- and polyethylene-reflected data for ^{3}He. The analytic error bars have overlap the sample method error bars for the organic scintillators and overestimate the relative uncertainty. Even better agreement is shown in the ^{3}He data and the analytic method again estimates relative uncertainties greater than the center of the sample error bars. Note that the overestimation increases for larger time differences; the trend could be due to accidental counts contributing more uncertainty than the correlated counts are, though further investigation is the subject of future work. Further note that analytic error bars are less noisy than those of the sample method and that relative uncertainty scales as $(\text{measurementtime})^{-1/2}$, as shown in Fig. 7. The relative uncertainties in the ^{3}He data are much lower than those of the organic scintillator data; the ^{3}He system had double the measurement time and an efficiency 10–100 times greater than that of the organic scintillator system. Precise efficiency ratios are not available because the organic scintillator system did not measure the heterogeneous assembly.

Weights are calculated such that uncertainty from the histograms can be propagated to the estimate of α and such that the fitting is more accurate. Weights for the organic scintillator measurements of the copper-reflected BeRP Ball are shown in Fig. 8. If the weights are noisy, a fit of the weights can be used instead. A sample fit is also shown in Fig. 8. Fig. 9 shows the improvement in accuracy due to weighting; note that this work chooses to take the simulated values of the prompt period from Ref. Hua et al. (2020) as the reference value.

The analytic error bars were used to construct weights, weighted fits were applied to the organic scintillator data, and uncertainty was propagated from the fit parameters to obtain an analytic standard deviation on the estimate of the prompt period, $1/\alpha$. A sample standard deviation of the prompt period is also obtained by taking the standard deviation of the prompt periods calculated from 20 one-minute measurements for the copper case, and 30 one-minute measurements for the tungsten and nickel cases. The two methods are compared in Fig. 10 and agree within one standard deviation.

7. Summary and conclusion

The theory of propagating uncertainty from histogram data to final estimates of the prompt neutron decay constant is rigorously developed in this paper. Additionally, two methods of estimating the uncertainty in the histogram data are described: the sample variance method (taking the variance of repeated experiments) and the analytic method. The analytic method is validated by comparison to the sample variance method. Note that the analytic estimate of the uncertainty is less noisy and more stable than that of the sample variance method. Therefore, it may be preferential to use the analytic method when long, redundant measurements are infeasible and hence when the sample variance method is unreliable. Future work includes investigating bootstrapping, another resampling modality of estimating the histogram error bars. In general, reducing the number of repeated measurements will reduce procedural and operational costs.

The validation is shown for both an organic scintillation detector-based system and a ^{3}He-based system, demonstrating that the analytic method is detection-system-agnostic. The histogram error bars are propagated to the uncertainty in the fit parameters by weighting the fit. In addition to correctly propagating uncertainty, weighting the fit improves the accuracy of prompt neutron decay constant estimates. Thus, fit algorithms should be weighted. Future work will use the weights and uncertainty analysis to determine fitting best-practices such as optimal bin widths, the length of the constant-only region, and optimal fitting ranges (initial and terminal time cuts).

CRediT authorship contribution statement

Michael Y. Hua: Conceptualization, Methodology, Software, Validation, Formal analysis, Investigation, Data curation, Writing - original draft, Visualization. **Jesson D. Hutchinson:** Conceptualization, Validation, Investigation, Resources, Writing - review & editing. **George E. McKenzie:** Investigation, Resources. **Brian C. Kiedrowski:** Methodology, Visualization. **Michael W. Liemohn:** Methodology, Writing - review & editing. **Shaun D. Clarke:** Writing - review & editing, Funding acquisition. **Sara A. Pozzi:** Writing - review & editing, Funding acquisition.

Declaration of Competing Interest

The authors declare that they have no known competing financial interests or personal relationships that could have appeared to influence the work reported in this paper.

Acknowledgments

This work was partially supported by the National Science Foundation Graduate Research Fellowship under Grant No. DGE-1256260, the Consortium for Verification Technology under Department of Energy National Nuclear Security Administration award number DE-NA0002534, the Consortium for Monitoring, Technology, and Verification under Department of Energy National Nuclear Security Administration award number DE-NA0003920, and the DOE Nuclear Criticality Safety Program, funded and managed by the National Nuclear Security Administration for the Department of Energy. Any opinion, findings, and conclusion or recommendations expressed in this material are those of the authors and do not necessarily reflect the views of any funding organization.

References

Albritton, D., Schmeltekopf, A., Zare, R., 1976. An introduction to the least-squares fitting of spectroscopic data 1.

Avery, R., 1958. Coupled fast-thermal power breeder. Nucl. Sci. Eng. 3 (2), 129–144. https://doi.org/10.13182/NSE58-A25455.

Bess, J., Hutchinson, J. Benchmark analysis of subcritical noise measurements on a nickel-reflected plutonium metal sphere.

Brooks, F., 1959. A scintillation counter with neutron and gamma-ray discriminators. Nucl. Instrum. Methods 4 (3), 151–163. https://doi.org/10.1016/0029-554X(59)90067-9.

Cohn, C.E., 1962. Reflected-reactor kinetics. Nucl. Sci. Eng. 13 (1), 12–17. https://doi.org/10.13182/NSE62-A26122.

Nuclear safeguards, security, and nonproliferation, in: J.E. Doyle (Ed.), Nuclear Safeguards, Security, and Nonproliferation, second ed., Butterworth-Heinemann, Boston, 2019.https://doi.org/10.1016/B978-0-12-803271-8.12001-6.

Feynman, R., DeHoffman, F., Serber, R., 1956. Dispersion of the neutron emission in U-235 fission. J. Nucl. Energy (1954) 3 (1) (1956) 64 – IN10.https://doi.org/10.1016/0891-3919(56)90042-0.

Feynman, R., DeHoffman, F., Serber, R. Statistical fluctuations in the water boiler and the dispersion of neutrons emitted per fission, LA-101, Los Alamos National Laboratory.

Feynman, R., DeHoffman, F., Serber, R. Intensity fluctuations of a neutron chain reactor, LADC-256, Los Alamos National Laboratory.

Hansen, G.E. The rossi alpha method, Los Alamos National Laboratory, Technical Report (LA-UR-85-4176).

Hua, M.Y., Hutchinson, J.D., McKenzie, G.E., Shin, T.H., Clarke, S.D., Pozzi, S.A., 2020. Derivation of the two-exponential probability density function for rossi-alpha measurements of reflected assemblies and validation for the special case of shielded measurements. Nucl. Sci. Eng. 194 (1), 56–68. https://doi.org/10.1080/00295639.2019.1654327.

Hua, M.Y., Bravo, C.A., MacDonald, A.T., Hutchinson, J.D., McKenzie, G.E., Kiedrowski, B.C., Clarke, S.D., Pozzi, S.A., 2020. Rossi-alpha measurements of fast plutonium metal assemblies using organic scintillators. Nucl. Instrum. Methods Phys. Res. Sect. A 959, 163507https://doi.org/10.1016/j.nima.2020.163507.

Hutchinson, J., Bahran, R., Cutler, T., Arthur, J., Nelson, M. Subcritical copper-reflected alpha-phase plutonium (SCRaP) measurements and simulations. In: M&C 2017 – International Conference on Mathematics & Computational Methods Applied to Nuclear Science & Engineering.

Hutchinson, J., McKenzie, G., Arthur, J., Nelson, M., Monage, W., 2017. Prompt neutron decay constant fitting using the rossi-alpha and feynman variance-to-mean methods. Trans. Am. Nucl. Soc. 117, 986–989.

Kuramoto, R., dos Santos, A., Jerez, R., Diniz, R., Bitelli, U., Madi Filho, T., Luis Veneziani, C., 2006. Rossi-α experiment in the IPEN/MB-01 research reactor: validation of two-region model and absolute measurement of β_{eff} and Λ.

Miller, L.F., Preston, J., Pozzi, S., Flaska, M., Neal, J., 2007. Digital pulse shape discrimination. Rad. Prot. Dosim. 126 (1–4), 253–255. https://doi.org/10.1093/rpd/ncm052.

Miller, E., Dennis, B., Clarke, S., Pozzi, S., Mattingly, J., 2011. Simulation of polyethylene-moderated plutonium neutron multiplicity measurements. Nucl. Instrum. Methods Phys. Res. Sect. A 652(1), 540–543, symposium on Radiation Measurements and Applications (SORMA) XII 2010.https://doi.org/10.1016/j.nima.2011.01.042.

Orndoff, J., 1957. Prompt neutron periods of metal critical assemblies. Nucl. Sci. Eng. 2 (4), 450–460.

Papoulis, A., 1984. Probability, Random Variables, and Stochastic Processes. McGraw-Hill, New York.

Polack, J., Flaska, M., Enqvist, A., Sosa, C., Lawrence, C., Pozzi, S., 2015. An algorithm for charge-integration, pulse-shape discrimination and estimation of neutron/photon misclassification in organic scintillators. Nucl. Instrum. Methods Phys. Res. Sect. A 795, 253–267. https://doi.org/10.1016/j.nima.2015.05.048.

Richard, B., Hutchinson, J. Nickel reflected plutonium metal sphere subcritical measurements, In: International Handbook of Evaluated Criticality Safety Benchmark Experiments [DVD]/Nuclear Energy Agency. - Paris: OECD Nuclear Energy Agency, (NEA;7328).

Richard, B., Hutchinson, J. Tungsten-reflected plutonium-metal-sphere subcritical measurements. In: International Handbook of Evaluated Criticality Safety Benchmark Experiments [DVD]/Nuclear Energy Agency. – Paris: OECD Nuclear Energy Agency, (NEA;7328).

Uhrig, R., Commission, U.A.E., 1970. Random Noise Techniques in Nuclear Reactor Systems. Ronald Press.